Chapter 3

Feed Perturbation Analysis of a Cylindrical Dielectric Resonator Antenna

3.1 Introduction

As discussed in chapter 1, a given feed mechanism is impedance matched to the DRA by adjusting the feed position relative to some reference position of the DRA, which for a CDRA is its center. When the magnitude of the reflection coefficient is minimum, ($|\Gamma_{in}|_{min}$) the impedance matching is said to have achieved. Now the DRA is glued or taped on the feed structure for detailed characterizations. This traditional approach may however result in a sub-optimum DRA design as it used the impedance matching as the sole criterion for choosing the feed point. In this chapter, it is demonstrated that for a CDRA operating at the $HEM_{11\delta}$ mode, fairly good impedance matching ($|\Gamma_{in}|_{min} < -10$ dB) at around the same resonant frequency can be achieved from more than one feed points. But for each feed point, the radiation properties of the mode also vary. This is due to the excitation of one or many higher order modes of the DRA by the particular feed mechanism, which is termed as the feed perturbation. The multi-polar nature of the unwanted DRA modes results in pattern distortion. The above aspects are investigated for a CDRA with respect to three common standard feed mechanisms – the microstrip line feed, the microstrip slot feed and the coaxial probe feed. In this chapter, for modeling the CDRA to perform the simulations, parameters of an available CDR and the materials are used, so that fabrication and experimental validation can be performed. The CDR has dielectric constant $\varepsilon_r = 24$, $tan\delta = 0.002$, diameter $2a = 19.43$ mm and height $h = 7.3$ mm ($a/h = 1.33$). For the feed modeling, readily available and cost effective FR4 substrate ($\varepsilon_r = 4$, $tan\delta = 0.02$, thickness = 1.6 mm) with double sided copper cladding is used.

3.2 The Feed Mechanisms

Feed mechanisms for DRAs (as for any RF device) are realized either as single ended feeds or differential feeds. Single ended feeds are simpler in construction and operation [31],[4], while differential feeds at the cost of tighter amplitude and phase balance of the feed currents, results in lower spurious (cross-polar) radiation [62],[63]. It is known that the hybrid modes of a DRA

radiates as multi-poles [8]. As discussed in chapter 1, the dominant broadside mode of an isolated cylindrical DRA designated as the $HEM_{11\delta}$ (approximated as TM_{110}) mode radiates like a horizontal magnetic dipole [8]. The feed mechanism designed for exciting the $HEM_{11\delta}$ mode is thus desired to couple maximum energy, only to the magnetic dipole and minimum energy to the lower and higher order multi-poles that may be excited by the feed. The relative strengths of constituent multi-pole components of the mode will thus depend on the feed point for a given feed mechanism.

Table 3.1 Design Parameters for the CDR and the Feed mechanisms

Parameter	Value
Common parameters	
CDR diameter, $2a$	19.43 mm
CDR height, h	7.3 mm
CDR ε_r, tanδ	24, 0.002
Substrate / ground plane size	115 mm side
Substrate / ground plane height	1.6 mm
Radial feed position, l_s	To be optimized
Microstrip line feed	
Substrate ε_r, tanδ	4, 0.02
Width of microstrip	3.22 mm
Microstrip slot feed	
Substrate ε_r, tanδ	4, 0.02
Width of microstrip	3.22 mm
Slot length	10 mm
Slot width	2 mm
Coaxial probe feed	
Probe length above the ground plane	7.3 mm
Probe diameter	1.64 mm
Coax outer diameter	5.5 mm
Dielectric medium inside the coax ε_r, tanδ	2.1,0.001

Choice of the wrong feed point of the DRA will thus results in a reduction of the purity of the desired mode, hence a deterioration of the DRA performance. Major performance parameters

of the DRA that are affected in this way are the symmetry of the radiation pattern and the level of the cross-polarized radiation. In order to analyze the above facts, a microstrip line, a microstrip slot and a coaxial probe, individually coupled to the same CDR are modeled using ANSYS HFSS. The design parameters of the CDRA employing the three feed mechanisms are shown in Table 3.1.

Before starting the modeling and simulation of the DRA with ANSYS HFSS, resonant frequency of the $HEM_{11\delta}$ mode CDRA (Table 3.1) can be computed by using closed form equations available in the literature as follows.

Coaxial fed CDRA [8]: $f_0 = \frac{6.324c}{2\pi a\sqrt{\varepsilon_r+2}}\left[0.27 + 0.36\left(\frac{a}{2h}\right) + 0.02\left(\frac{a}{2h}\right)^2\right], 0.4 \leq \frac{a}{h} \leq 6$ …(3.1)

Slot fed CDRA[21]: $f_0 = \frac{c}{2\pi a\sqrt{\varepsilon_r}}\left[1.71 + 2.0\left(\frac{a}{2h}\right) + 0.1578\left(\frac{a}{2h}\right)^2\right], 20 \leq \varepsilon_r \leq 24$ …(3.2)

Equations 3.1 and 3.2 give the resonant frequency as 3.16 GHz and 3.12 GHz respectively for the given CDRA. For microstrip fed CDRA there exists no such closed form equations, so either of the above equations may be used.

3.2.1 Microstrip line feed

Microstrip line offers simplicity in the design, fabrication and impedance matching and can be used for exciting the $HEM_{11\delta}$ mode of a cylindrical DRA [19]. A 50 Ω microstrip line terminated in an open circuit is designed using a copper coated dielectric substrate to which the DRA is proximity coupled. Microstrip line design parameters for 50 Ω are shown in Table 3.1. Symmetric positioning of the DR with respect to the open end of the line is very important for setting the polarization of the $HEM_{11\delta}$ mode in the direction of the microstrip line. The ε_r of the CDR being high (ε_r = 24) eases the impedance matching to the 50 Ω feed that was made on a low (ε_r = 4) substrate [17]. The schematic diagram of the microstrip fed CDRA is shown in the Fig. 3.1. The DRA is placed on the top of the line so that the open end extends under the CDRA by a length l_s, which decides the feed point. The feed parameter l_s is varied from 0 mm to 8 mm and the magnitude of the input reflection coefficient $|\Gamma_{in}|$ are recorded. The antenna characteristics are then extracted at the minimum $|\Gamma_{in}|$ frequency of f_0 and are shown in Table

3.2. Peak CDRA gains from the radiation patterns in the two principal planes (E-plane and H-plane) are noted between the $\pm 90^0$ elevation about the boresight ($\theta = 0^0$).

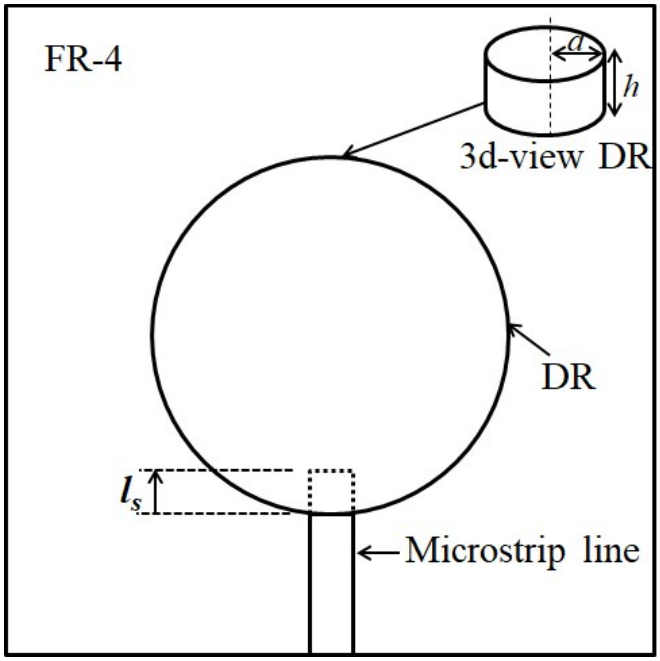

Fig. 3.1 Schematic of microstrip line fed CDRA

Table 3.2 CDRA characteristics: Microstrip feed for various feed points (*l*s in Fig. 3.1)

l_s (mm)	f_0 (GHz)	$\|\Gamma_{in}\|$ (dB)	% Band width	Max. co-polar gain (dB)		Max. cx-polar gain (dB)	
				E-plane	H-plane	E-plane	H-plane
< 2	No coupling ($\|\Gamma_{in}\|$ = 0 dB)						
2	3.47	–50	6.49	5.29	4.59	–34	–22
4	3.52	–24	6.81	5.24	4.61	–35	–21
6	3.55	–35	6.67	5.21	4.57	–38	–19
8	3.57	–13	3.92	5.70	4.08	–43	–14

3.2.2 Microstrip slot feed

The CDR is placed directly on top of the slot made on the ground plane with its center coinciding with the center of the slot [21]. The 50 Ω microstrip is running on the backside of the substrate that couples to the CDR through the slot, as shown in Fig. 3.2.

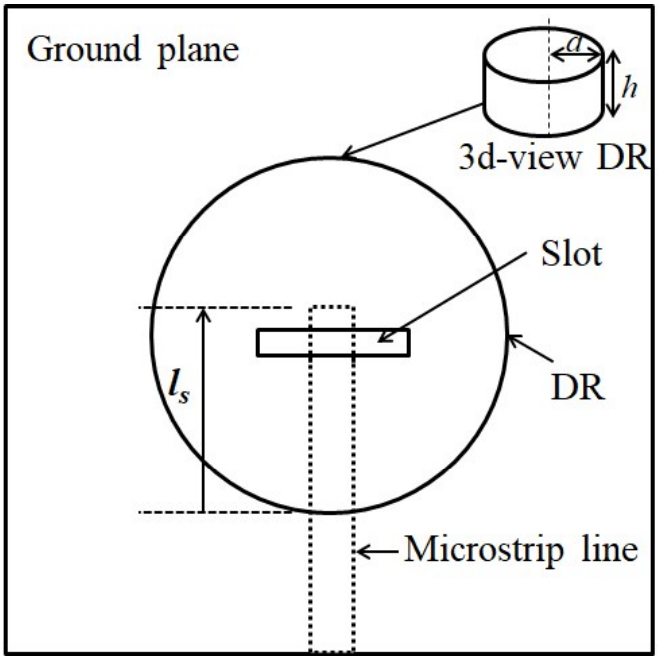

Fig. 3.2 Schematic of microstrip slot fed CDRA

Table 3.3 CDRA characteristics: Microstrip slot feed, for various feed points (l_s in Fig. 3.2)

l_s (mm)	f_0 (GHz)	$\|\Gamma_{in}\|$ (dB)	% Band width	Max. co-polar gain (dB)		Max. cx-polar gain (dB)	
				E-plane	H-plane	E-plane	H-plane
< 12	No coupling ($\|\Gamma_{in}\|$=0 dB)						
12	2.78	–46	2.37	5.39	5.39	–36	–26
14	2.68	–30	1.83	5.62	5.62	–35	–29
33	2.83	–27	2.26	5.41	5.39	–42	–30
45	2.69	–22	1.84	4.80	4.71	–44	–33
46	2.67	–23	2.14	4.74	4.65	–43	–34

Detailed design parameters of the slot feed are shown in Table 3.1. The length l_s of the microstrip open end as shown in Fig. 3.2 is adjusted to achieve impedance matching. Table 3.3 shows the antenna properties for different l_s for the slot fed CDRA.

3.2.3 Coaxial probe feed

The schematic model of the coaxial probe fed CDRA is shown is Fig. 3.3 which is based on the design parameters given in Table 3.1.

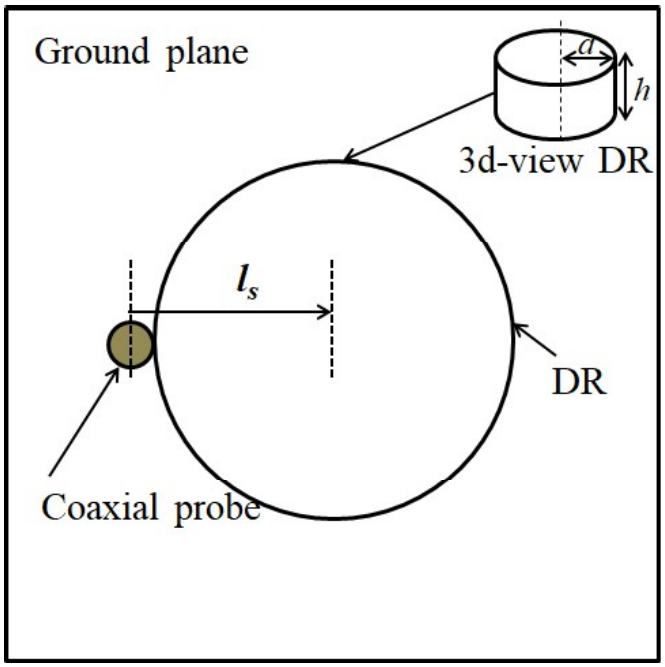

Fig. 3.3 Schematic of coaxial probe fed CDRA

Table 3.4 CDRA characteristics: Coaxial probe feed, for various feed points (l_s in Fig. 3.3)

l_s (mm)	f_0 (GHz)	$\|\Gamma_{in}\|$ (dB)	% Band width	Max. co-polar gain (dB)		Max. cx-polar gain (dB)	
				E-plane	H-plane	E-plane	H-plane
< 0	No coupling						
0	3.08	–38	3.02	6.10	6.09	–39	–31
1	3.09	–15	3.01	6.00	5.96	–39	–27
6	3.06	–15	2.75	6.19	6.19	–21	–18
7	3.07	–41	2.83	6.15	6.00	–40	–13

The CDR is mounted directly on top of the metallic ground plane, through which the probe of a 50 Ω coaxial line is extended upward. The probe length above the ground plane is chosen in order to achieve the best impedance matching for any feed point decided by length l_s. Antenna characteristics for this arrangement are tabulated in Table 3.4.

3.3 Analysis of Simulation Results

3.3.1 Effect of the Feed-point on the CDRA performance

For the microstrip fed CDRA, as shown in Table 3.2, an impedance matching with $|\Gamma_{in}| < -10$ dB is achieved when $l_s > 0$ mm, i.e the strip end overlaps with the CDR. As l_s increases, the resonant frequency keeps increasing at smaller steps while the percentage bandwidth first increases then decreases. The reflection coefficient also varies cyclically with the minimum value at $l_s = 2$ mm and the maximum value at $l_s = 8$ mm. Peak gains in the E-plane and the H-plane deviates from each other as l_s is increased, implying an asymmetry of the radiation pattern. The cross-polarized gain in the H-plane also increases with l_s in a fashion similar to that observed with the pattern asymmetry. The lowest impedance matching of $|\Gamma_{in}|$ of –13 dB, the highest level of pattern asymmetry of 1.62 dB and the highest cross-polar gain of –14 dB are achieved when the tip of the microstrip is nearer to the center of the CDR i.e, at $l_s = 8$ mm. Thus it can be concluded that geometrically asymmetric feeds such as the microstrip line excites the $HEM_{11\delta}$ mode with less mode purity, implying the presence of higher levels of higher order multi-polar components.

As shown in Table 3.3, For the microstrip slot fed CDRA, at feed point $l_s < 12$ mm, the strip is not completely crossing the slot, hence results in insufficient coupling to the CDR. Owing to the high inductance of the narrow slot, the tolerances of a slot-fed CDRA for impedance matching are much tighter than that of the microstrip feed. The resonant frequency and bandwidth follow cyclic behavior with l_s. It can be noted that for all values of l_s, the radiation pattern is nearly symmetric with reduced cross-polarized radiation in the H-plane. It can also be noted from Table 3.3 that as l_s gets higher, both the impedance matching and the cross-polarization level get lower, a trend contrary to that observed in the case of the microstrip fed CDRA.

In the case of the coaxial probe fed CDRA, feed point $l_s < 0$ mm, doesn't cause any physical contact between the probe and the CDRA hence no impedance matching is achieved. At $l_s = 0$ mm the excellent impedance matching of $|\Gamma_{in}| = -38$ dB and the least cross-polarization level of –31 dB are observed. When the probe location is closer to the center of the CDR, i.e, $l_s = 7$ mm, the H-plane cross-polarization reaches its maximum of –13 dB. It is also observed that the frequency sensitivity of the probe fed CDRA is the least among the three.

3.3.2 Comparison among the feed mechanisms for the optimum feed point

Analysis of the results in Tables 3.2 – 3.4 indicates that the performance of the CDRA excited in the $HEM_{11\delta}$ mode depends on the particular feed mechanism also for a given CDR geometry and material properties. For the microstrip slot and the coaxial probe feeds, the CDRA is placed directly on the metallic ground plane, hence by image theory, effective CDR height is double the actual height (~2*h*). This is however not true for a microstrip feed as the CDR is separated from the ground plane by the substrate. Hence the effective CDR height doesn't get doubled and the resonant frequency is higher than that for the other two feeds. Also for the same feed, the presence of the dielectric spacer (substrate) between the CDR and the ground also reduces the cavity effect, hence results in a lower *Q*-factor and a wider bandwidth of all the three feeds. Presence of the finite substrate loss ($\tan\delta = 0.02$) further reduces the *Q*-factor, as well as reduces the CDRA gain for the microstrip feed.

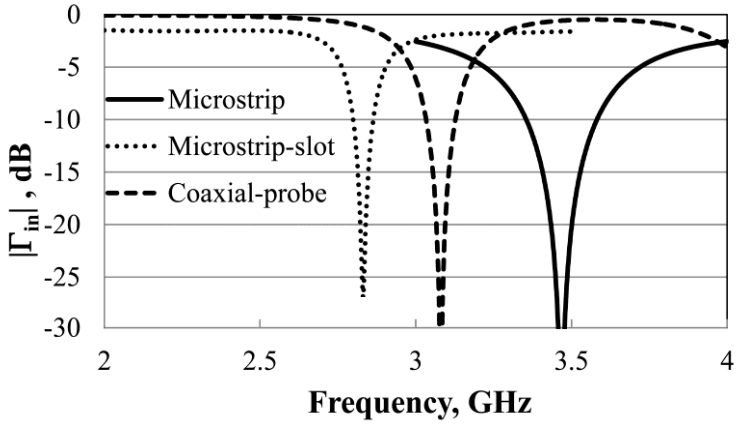

Fig. 3.4 Reflection coefficients of the CDRA employing different feeds. (Microstrip, $l_s = 2$ mm, Microstrip slot, $l_s = 33$ mm, Coaxial probe, $l_s = 0$ mm)

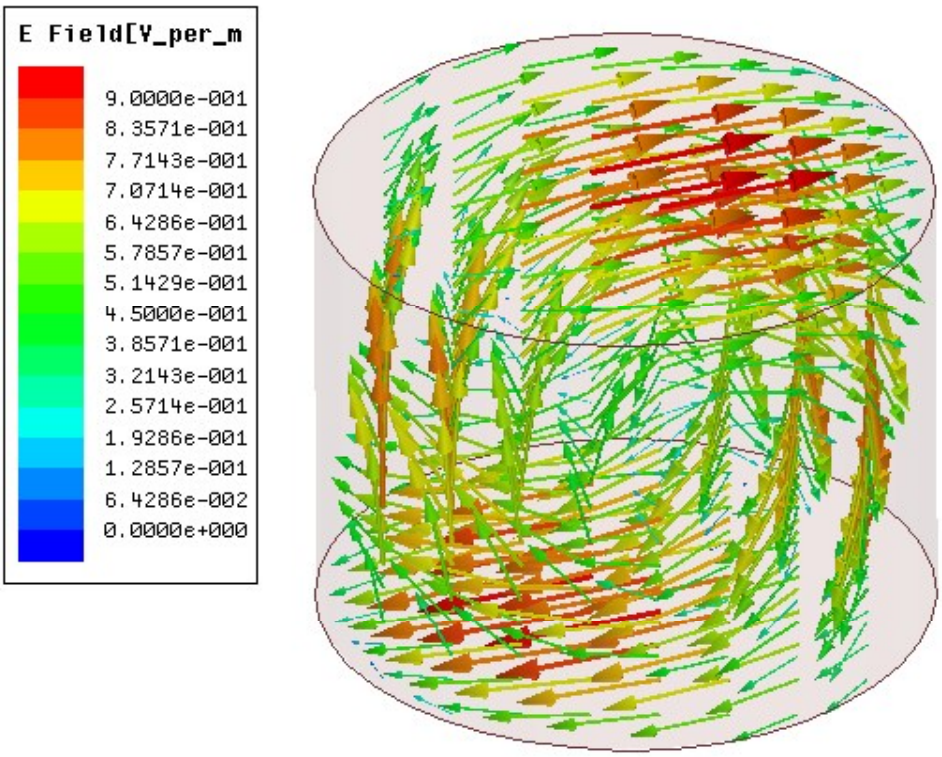
E Field[V_per_m
9.0000e-001
8.3571e-001
7.7143e-001
7.0714e-001
6.4286e-001
5.7857e-001
5.1429e-001
4.5000e-001
3.8571e-001
3.2143e-001
2.5714e-001
1.9286e-001
1.2857e-001
6.4286e-002
0.0000e+000

(a)

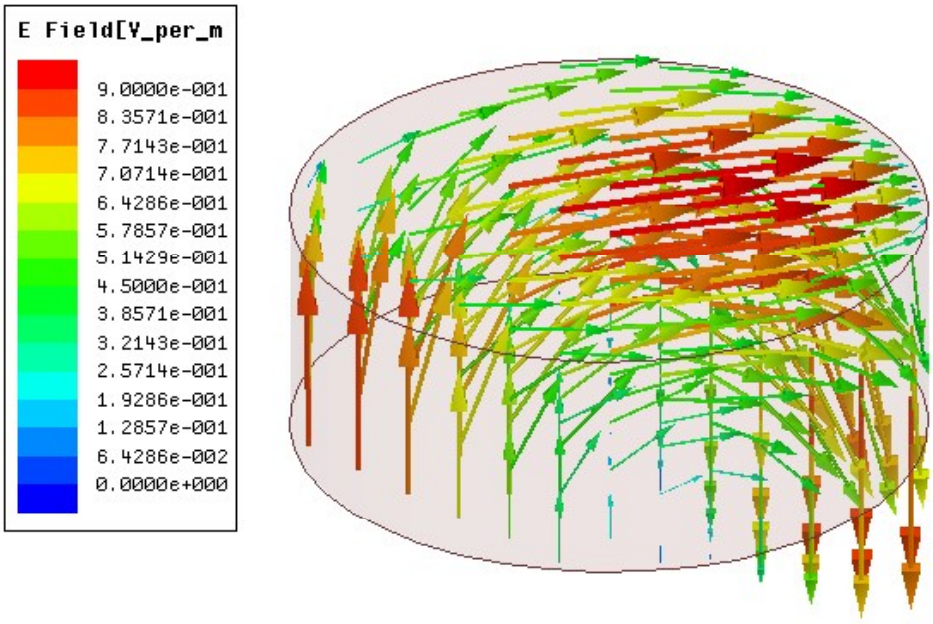
E Field[V_per_m
9.0000e-001
8.3571e-001
7.7143e-001
7.0714e-001
6.4286e-001
5.7857e-001
5.1429e-001
4.5000e-001
3.8571e-001
3.2143e-001
2.5714e-001
1.9286e-001
1.2857e-001
6.4286e-002
0.0000e+000

(b)

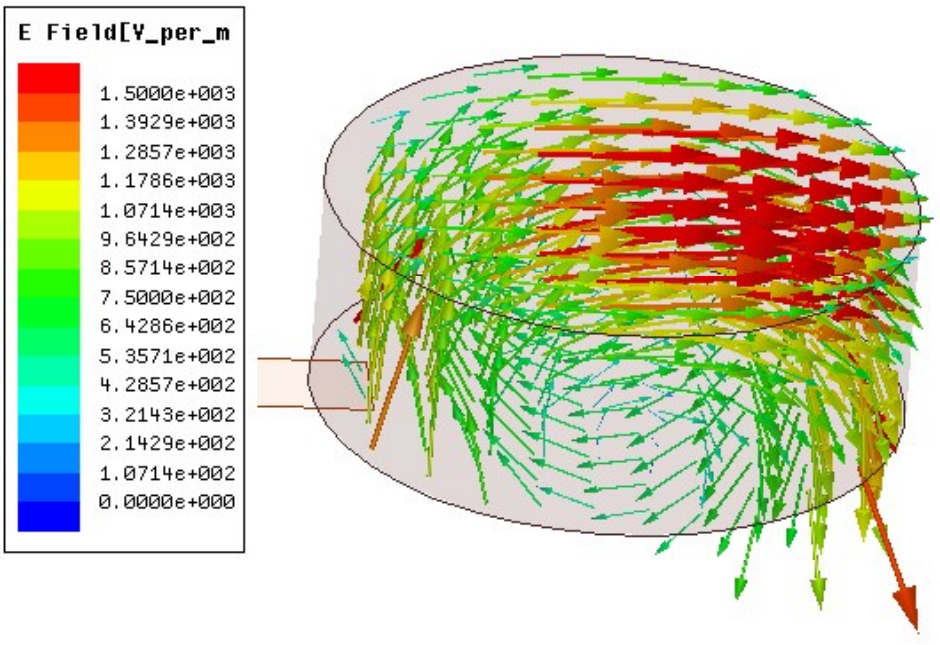
E Field[V_per_m
1.5000e+003
1.3929e+003
1.2857e+003
1.1786e+003
1.0714e+003
9.6429e+002
8.5714e+002
7.5000e+002
6.4286e+002
5.3571e+002
4.2857e+002
3.2143e+002
2.1429e+002
1.0714e+002
0.0000e+000

(c)

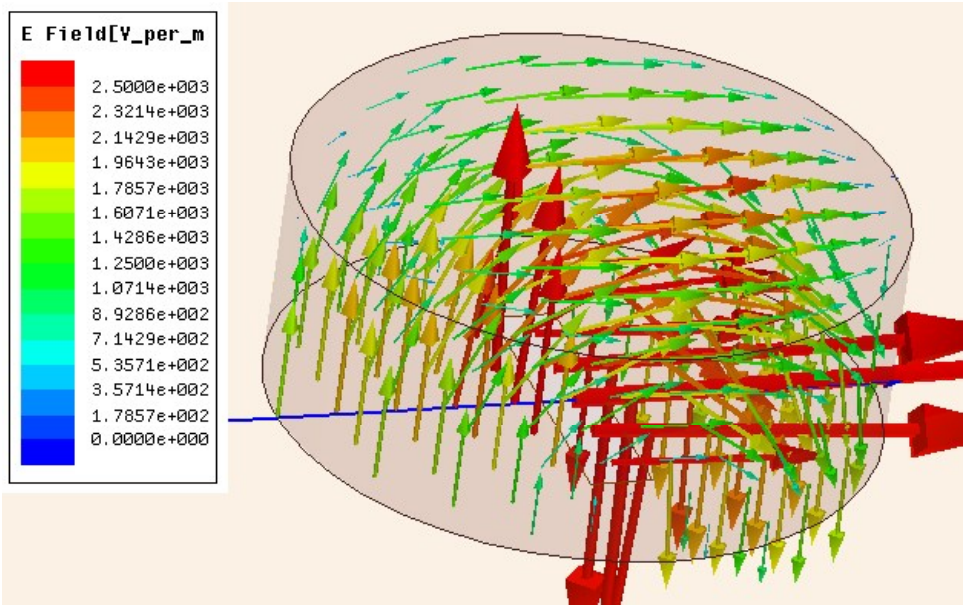
E Field[V_per_m
2.5000e+003
2.3214e+003
2.1429e+003
1.9643e+003
1.7857e+003
1.6071e+003
1.4286e+003
1.2500e+003
1.0714e+003
8.9286e+002
7.1429e+002
5.3571e+002
3.5714e+002
1.7857e+002
0.0000e+000

(d)

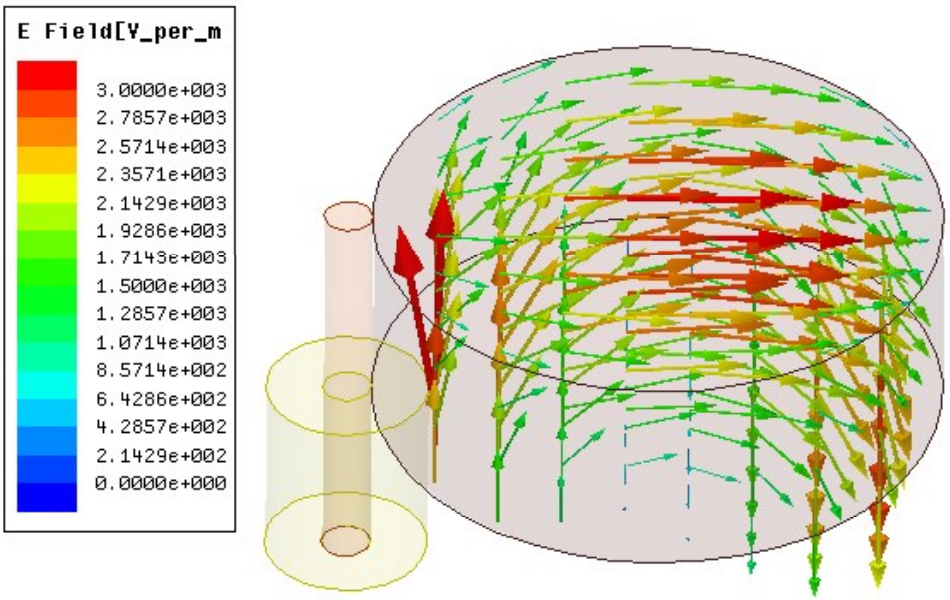

(e)

Fig. 3.5. The near-field distribution (E-field) of the $HEM_{11\delta}$ mode in the CDR for various feed boundary conditions: (a) Isolated CDR of diameter 2*a* and height 2*h* (b) CDR of diameter 2*a* height *h* kept on a ground plane (c) Microstrip fed CDR (2*a*, *h*) (d) Microstrip slot fed CDR (2*a*, *h*) (e) Coaxial probe fed CDR (2*a*, *h*)

For the slot feed, the effective feed point inductance is much higher than that for the other two feeds, which causes the resonant frequency of the CDRA to be the lowest of the three. The radiation pattern for the slot feed is highly symmetric, indicated by equal boresight gains in E and H-planes. A symmetric radiation pattern may also be correlated with a lower cross-polarized radiation in the H-plane as indicated in the tables 3.2–3.4. Thus in terms of the cross-polarization level, the slot feed is the best while the microstrip feed is the worst. Fig. 3.5 shows the electric field distribution (ANSYS HFSS) of the $HEM_{11\delta}$ mode in the CDR for various source conditions. Fig 3.5 (a) and (b) respectively signifies the isolated CDR of height = 2*h* and a CDR of height *h* placed on the ground plane. In the above cases, the resonant frequencies are 3.03 GHz for the taller CDR and 3.05 GHz for the shorter one, implying the image equivalence between the isolated and the practical conditions. In Fig 3.5 (c)–(e) the electric field distribution for the microstrip feed (3.47 GHz), slot feed (2.83 GHz) and the coaxial probe feed (3.08 GHz)

are shown. It can be observed that the resonant frequency is around 3 GHz for all the different cases, which also matches with the closed form value as per equations (3.1) and (3.2).

3.3.3 Selection of the optimum feed-point

Based on the above discussions, it can be inferred that for both the microstrip and the probe feeds (Table 3.2 and 3.4 respectively) the feed point (l_s) is preferred to be as close to the edge of the CDRA as possible, for the desired mode to be excited with lesser spurious (multi-polar) components. For the slot feed (Table 3.3), for every value of l_s, the mode symmetry is maintained, indicating very less spurious components in the mode. For any feed mechanism, the E-plane cross-polar gain is below ~ –30 dB for most of the feed points and the H-plane co-polar pattern is more or less symmetric. Thus, for the microstrip feed, slot feed and the coaxial feed, l_s = 2 mm, 33 mm and 0 mm respectively are chosen as optimum feed points. Fig. 3.4 and Fig. 3.6 show the reflection coefficient and the radiation patterns respectively for the best feed designs with a compromise among the impedance matching, bandwidth, pattern symmetry and cross-polar levels. As indicated in Fig. 3.6, the microstrip fed CDRA and the coaxial probe fed CDRA have more or less similar H-plane cross-polar distributions which maximizes within $\pm 90^0$ about the boresight with a null at the boresight.

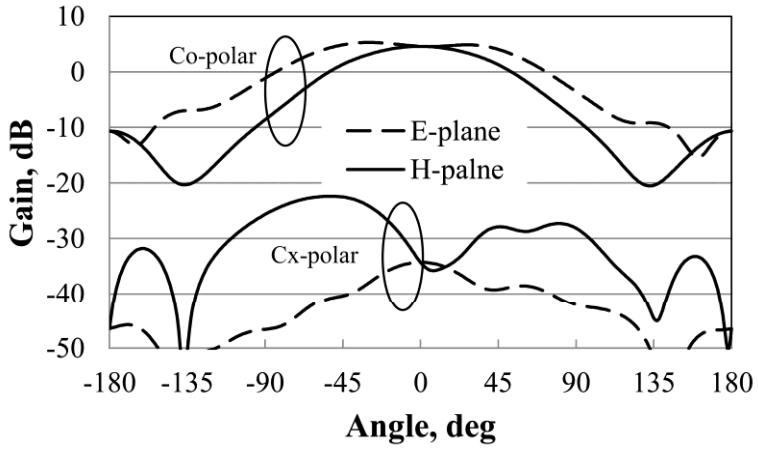

(a) Microstrip fed CDRA

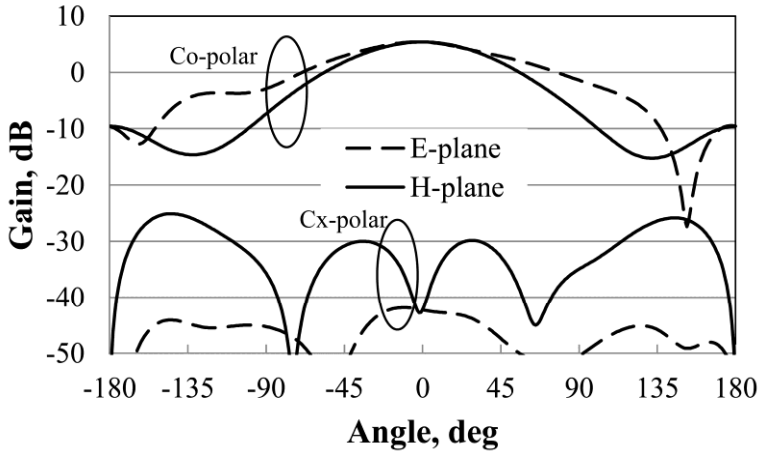

(b) Microstrip Slot fed CDRA

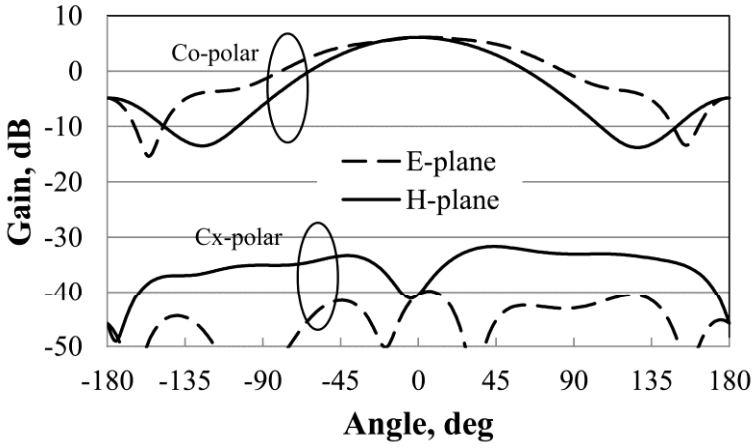

(c) Coaxial probe fed CDRA

Fig. 3.6 Simulated radiation pattern of the CDRA with different feeds. (Microstrip, l_s = 2 mm, Microstrip slot, l_s = 33 mm, Coaxial probe, l_s = 0 mm)

On the other hand, for the slot-fed CDRA, maximum H-plane cross-polar radiation occurs within $\pm 90^0$ about the back lobe direction. For the slot fed CDRA, presence of the three nulls in the H-plane cross-polar pattern within $\pm 90^0$ to the boresight imply the absence of those multi-polar components which are present in the microstrip and the coaxial-fed CDRAs.

Table 3.5 Comparison of the CDRA Performance for the three different feed mechanisms using ANSYS HFSS and CST Microwave studio (MWS)

(a) Microstrip fed CDRA, l_s = 2 mm							
Simulation Tool	f_0 (GHz)	$\|\Gamma_{in}\|$ (dB)	% Band width	Max. co-polar gain (dB)		Max. cx-polar gain (dB)	
				E-plane	H-plane	E-plane	H-plane
HFSS	3.47	–50	6.49	5.29	4.59	–34	–22
MWS	3.43	–37	6.60	6.35	5.41	–35	–18
(b) Microstrip slot fed CDRA, l_s = 33 mm							
Simulation Tool	**f_0 (GHz)**	**$\|\Gamma_{in}\|$ (dB)**	**% Band width**	**Max. co-polar gain (dB)**		**Max. cx-polar gain (dB)**	
				E-plane	**H-plane**	**E-plane**	**H-plane**
HFSS	2.83	–27	2.26	5.41	5.39	–42	–29
MWS	2.80	–27	2.38	6.64	6.63	–43	–23
(c) Coaxial-probe fed CDRA, l_s = 0 mm							
Simulation Tool	**f_0 (GHz)**	**$\|\Gamma_{in}\|$ (dB)**	**% Band width**	**Max. co-polar gain (dB)**		**Max. cx-polar gain (dB)**	
				E-plane	**H-plane**	**E-plane**	**H-plane**
HFSS	3.08	–38	3.02	6.10	6.09	–39	–31
MWS	3.07	–33	3.08	6.29	6.29	–44	–30

Performance of the optimum design for each feed type is cross-verified with CST Microwave Studio (MWS) and the results are furnished in Table 3.5. The table shows reasonable agreement between the two simulators for all the feed mechanisms. The resonant frequency and bandwidth are matching very well between the simulation tools. For the planar feeds (microstrip and slot), the gains in the E-plane and the H-plane vary by ~ 1 dB for either simulator. However, there is a mismatch of ~ 1 dB in the gain between the two simulation tools in the case of the planar feeds which is very small for the coaxial feed.

3.4 Prototypes and Measurement

The microstrip line and microstrip slot feeds are fabricated using FR-4 substrate. The coaxial probe feed is also fabricated using FR-4 substrate, with its top and the bottom metallizations soldered together along the edges. This was done for reducing the antenna weight to help mounting and alignment, which otherwise is difficult with a thick metal sheet. Fabricated feed mechanisms are shown in Fig. 3.7.

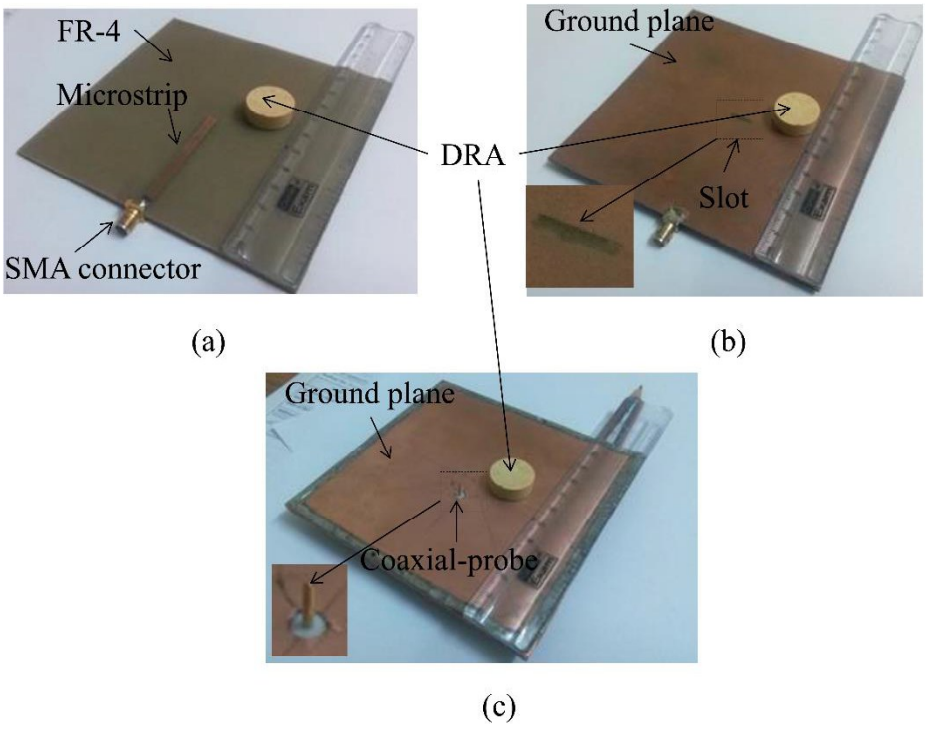

Fig. 3.7 Fabricated feed mechanisms (a) Microstrip (b) Microstrip slot (c) Coaxial probe

Measurements of the CDRAs are carried out in an anechoic chamber. Measured reflection coefficients for the three feed mechanism are shown in the Fig. 3.8 and the radiation patterns in Fig. 3.9, both in comparison with the respective simulated results. Important characteristics extracted from Fig. 3.8 and 3.9 are shown in Table 3.6. As shown, measured resonant frequencies and bandwidths closely agree with the simulated results. Eventhough the absolute values differ among simulation and measurement, relative variation from feed to feed follows the same trend as observed in simulations. Impedance matching and bandwidth are the highest with the microstrip feed while the same is the lowest with the slot feed. Similarly, the highest

gain is for the probe fed CDRA and the lowest for the microstrip fed CDRA. Pattern symmetry is well maintained by both the microstrip slot and the coaxial probe feeds over the upper hemisphere, as observed in simulations. However, in contrary to what is seen in simulation, the measured peak cross-polar levels (normalized with peak co-polar level) do not show much variation from feed to feed. This is because, accurate measurement of weak cross-polar radiation is difficult and is highly sensitive to alignment and other experimental errors [64]. Present measurements involved a good amount of manual positioning and alignment of the CDRA, hence the mismatch in the measured cross-polar results is expected.

Table 3.6 Comparison of the measured CDRA performance among the feed mechanisms

Feed type	l_s(mm)	f_0 (GHz)	$\|\Gamma_{in}\|$ (dB)	% Band width	Max. gain (dB)	Max. Cx-polar level (dB)
Microstrip	2	3.41	–56	6.3	4.39	–23
Microstrip-slot	33	2.86	–19	1.96	4.77	–24
Coaxial-probe	0	3.10	–39	3.27	5.81	–21

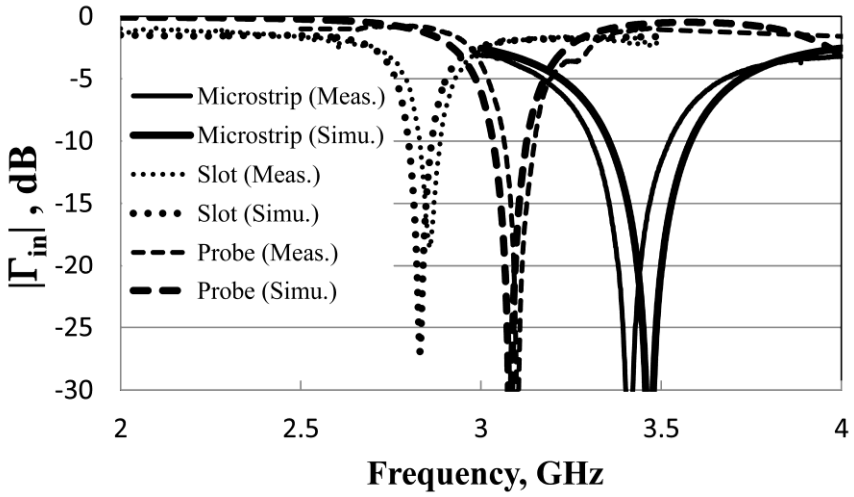

Fig. 3.8 Measured vs simulated reflection coefficients of the CDRA with three different feeds (Microstrip l_s = 2 mm, Microstrip slot l_s = 33 mm, Coaxial-probe l_s = 0 mm)

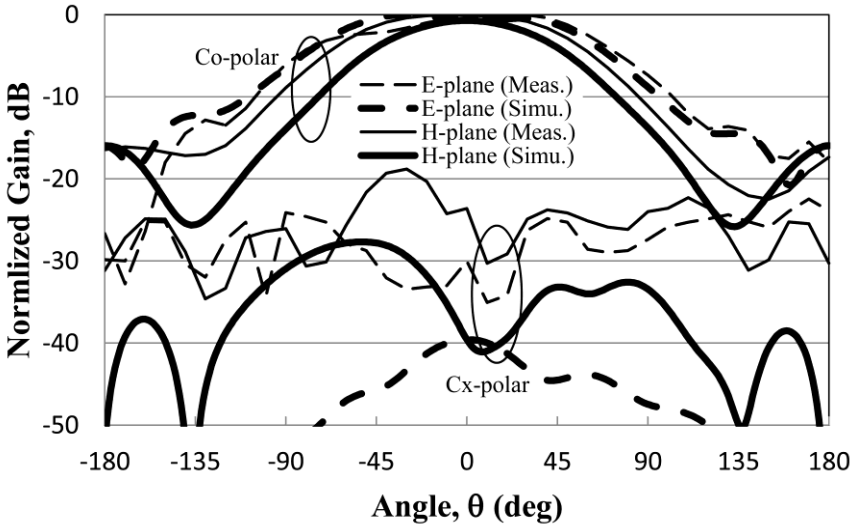

(a) Microstrip fed CDRA

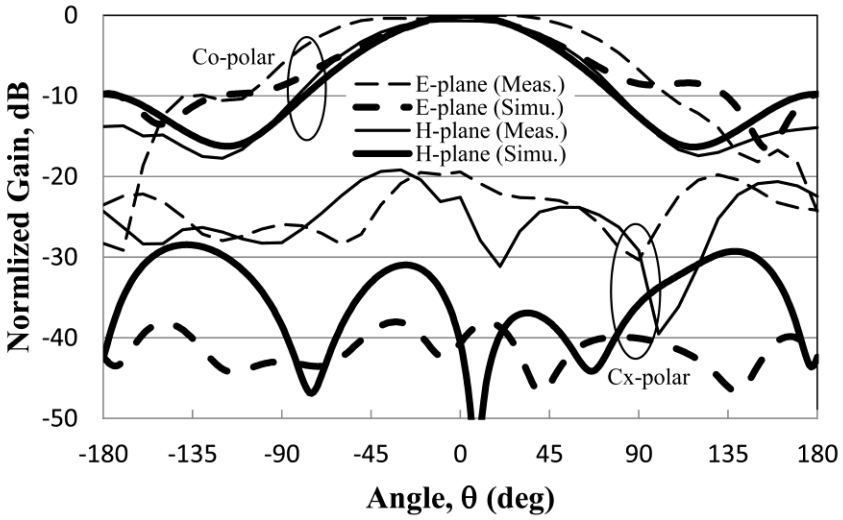

(b) Microstrip Slot fed CDRA

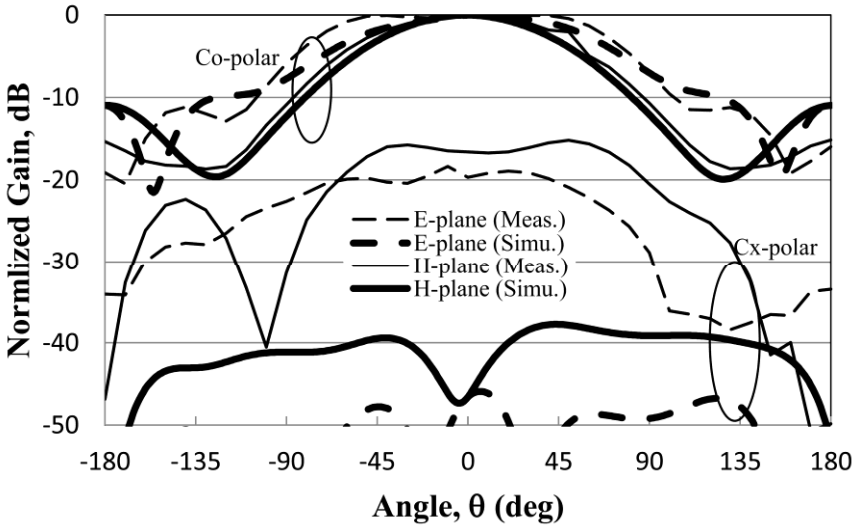

(c) Coaxial probe fed CDRA

Fig. 3.9 Measured vs simulated radiation patterns (normalized) of the CDRA with different feeds. (Microstrip, l_s = 2 mm, Microstrip slot, l_s = 33 mm, Coaxial probe, l_s = 0 mm)

3.5 Identification of the perturbing higher order mode

To identify the higher order mode(s) that is excited by the feed perturbation, the microstrip fed CDRA is considered, because in the previous analysis, it was giving the highest level of cross-polarization (Table 3.5). The near-field H-field plots inside the CDR volume for two different matching lengths l_s = 2 mm and 8 mm, generated by HFSS are shown in Fig. 3.10. From Fig. 3.10 (a–b), the mode can be identified readily as the $HEM_{11\delta}$ mode by comparing with standard results in [16]. Now for l_s = 2 mm, the maximum H-field (red colored lines) is found at the center of the CDR, while for l_s = 8 mm, the maximum field is shifted downward towards the feed. This gives the primary sign of a higher feed perturbation for longer matching lengths. Alternatively, the above downward shift signifies the presence of a multi-polar field which is stronger away from the center of the CDR. If the H-field shown in Fig. 3.10 (b) is animated for various RF phases, at a certain phase ($\omega t = 150^0$ for l_s = 2 mm and $\omega t = 40^0$ for l_s = 8 mm), some significant field around the strip region is clearly visible as shown in Fig. 3.10 (c). Further examination of this plot indicates that the H-field in the lower half of the CDR (near the strip) is 180^0 out of phase with the field in the upper half.

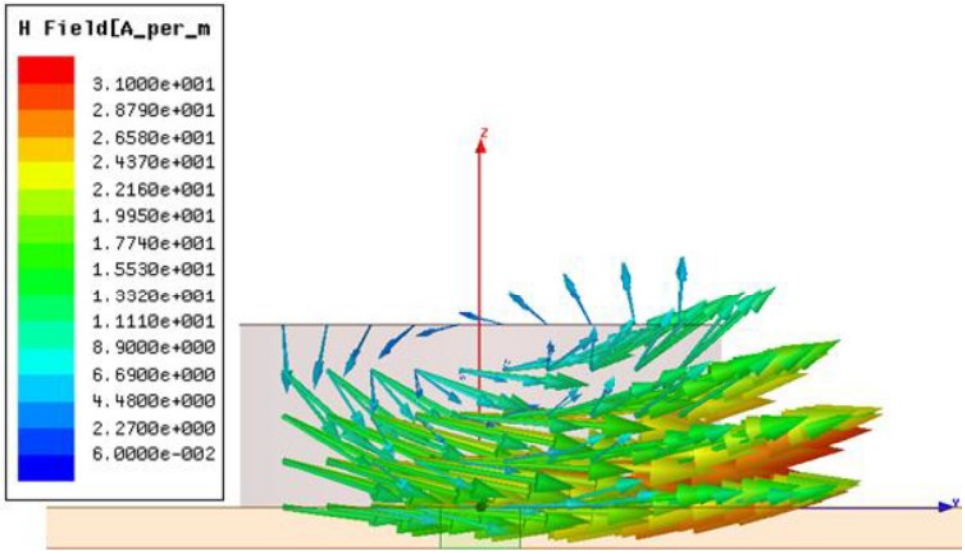

(a) Side-view for l_s= 2 mm at 60^0

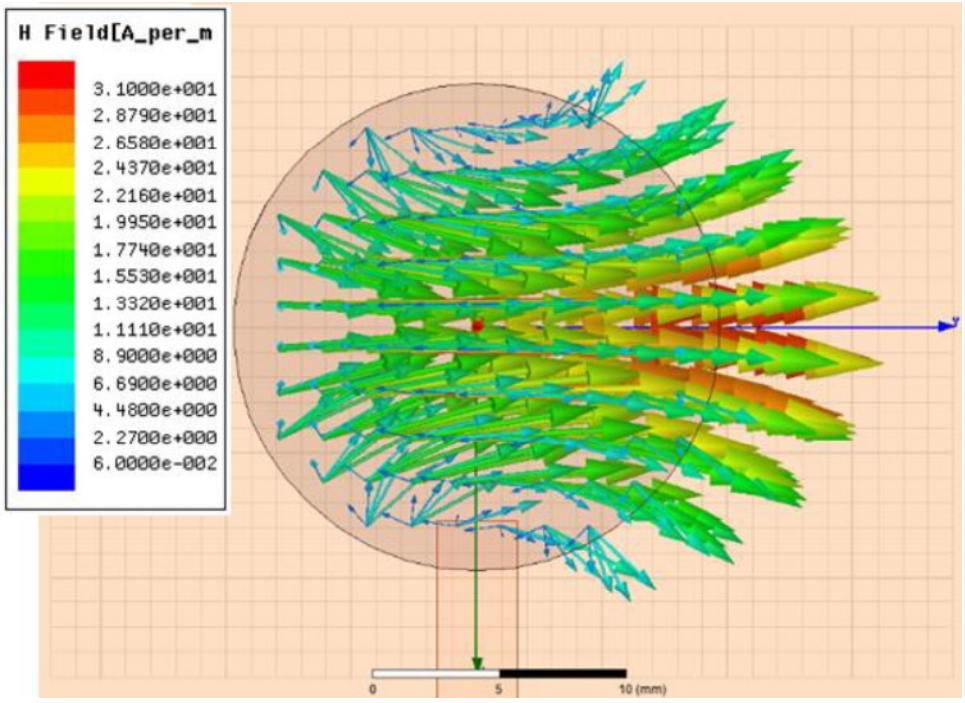

(b) Top-view for l_s= 2 mm at 60^0

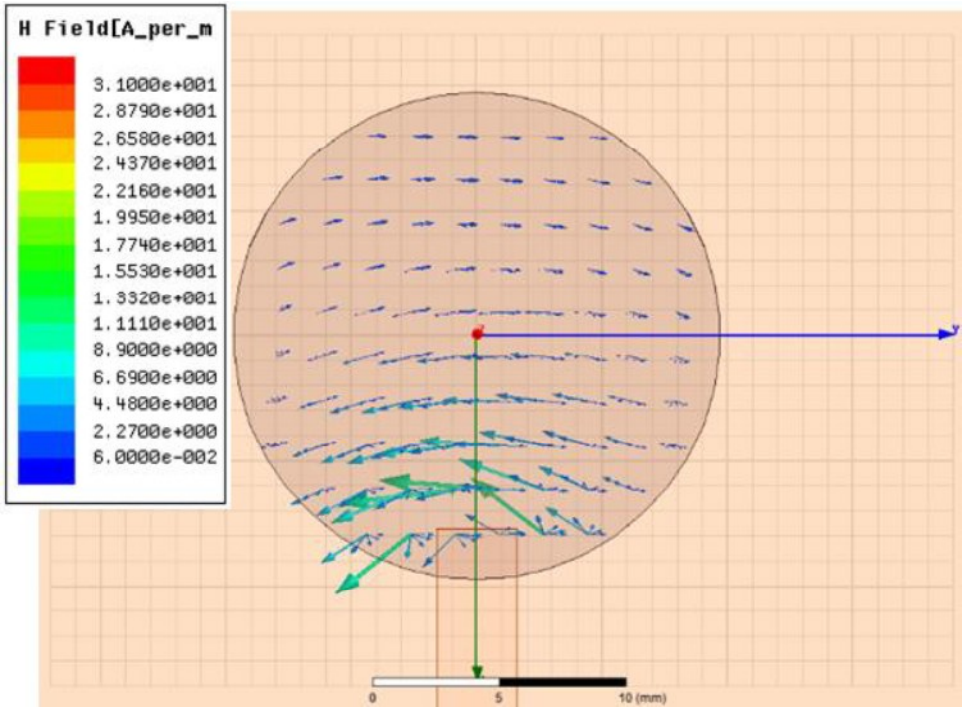

(c) Top-view for l_s= 2 mm at 150^0

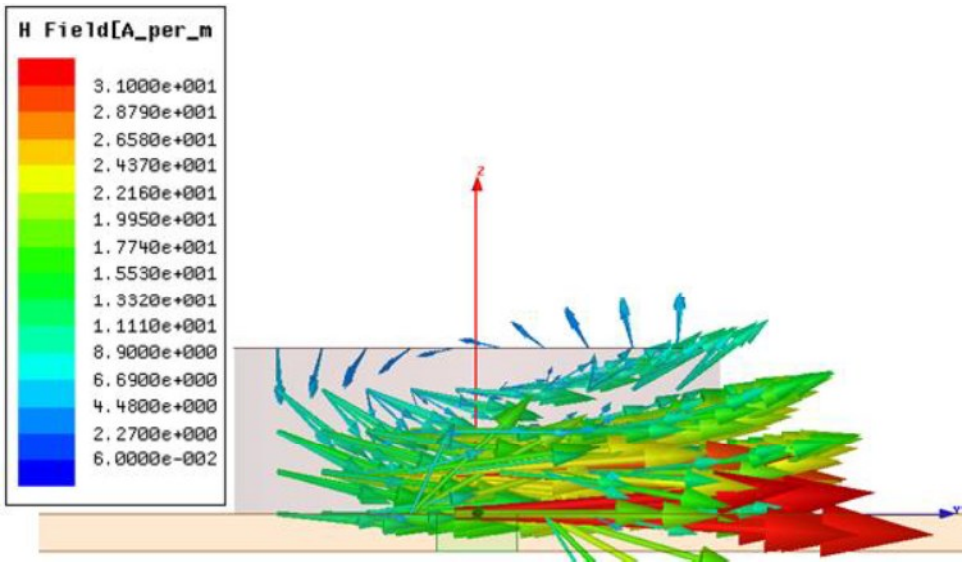

(a) Side-view for l_s= 8 mm at 130^0

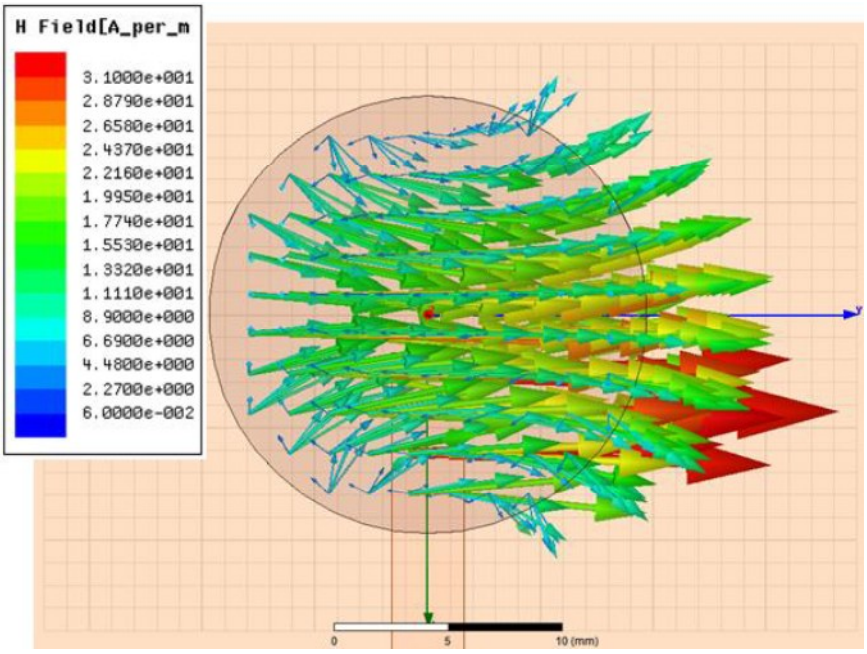

(b) Top-view for l_s= 8 mm at 130^0

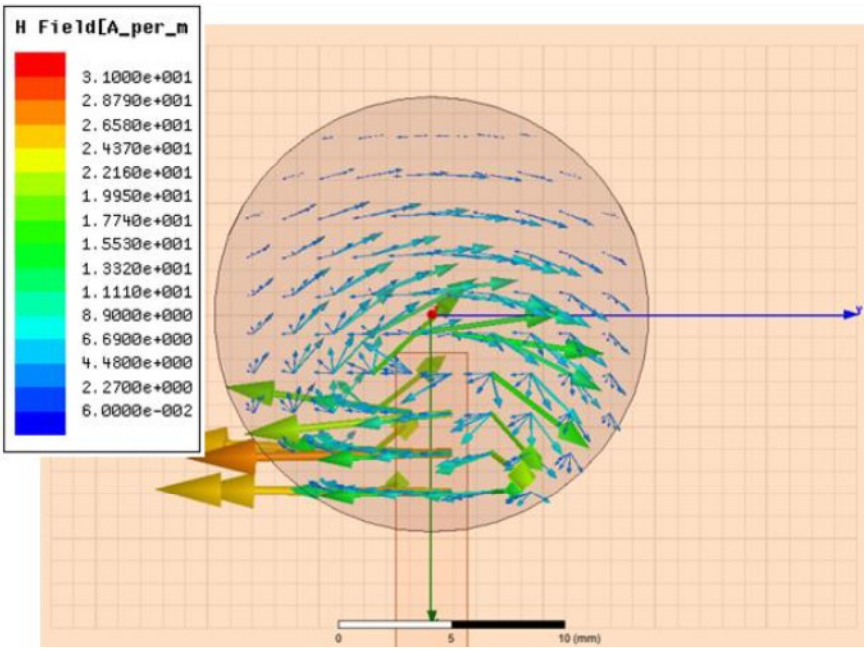

(c) Top-view for l_s= 8 mm at 40^0

Fig. 3.10 Near-field distribution (H-field) of the CDRA for l_s = 2 mm and 8 mm respectively at specific RF phases. (All plots use the same 0–31 A/m range)

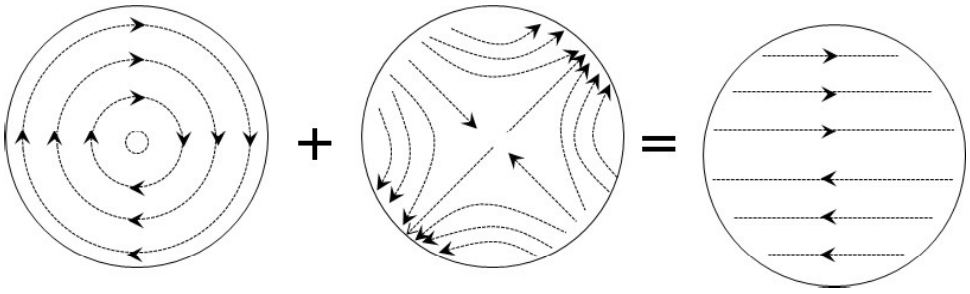

Fig. 3.11 Illustration of forming a mixed modal field pattern (H-field) by combining the $TM_{01\delta}$ and the $HEM_{21\delta}$ modal patterns as observed in Fig. 3.10(c)

From the eigen mode plots of the CDR [7], the modes that are having strong tangential H-field away from the center of the CDR can be identified as $TM_{01\delta}$ and $HEM_{21\delta}$ modes. As the above eigen modes are closer in frequency [7], they are likely to be excited simultaneously by the feed. If the eigen field distributions of the $TM_{01\delta}$ and $HEM_{21\delta}$ modes are combined, assuming equal strengths of both, the resulting field pattern shown in Fig. 3.11 looks very much like what is shown by HFSS (Fig. 3.10 (c) at l_s = 8 mm). From the above analysis, it can be concluded that a strip of longer matching length (l_s) excites both $TM_{01\delta}$ and $HEM_{21\delta}$ modes more strongly as the maxima of these modes are more likely to coincide with a longer strip. Measured CDRA characteristics for various matching lengths are furnished in Table 3.7 which exhibit identical trend as observed in simulations (Table 3.2). In the table, the gain asymmetry is calculated as the difference in the peak gains of the E-plane and the H-plane patterns, while the cross-polar level as the peak cross-polar level in the H-plane (E-plane cx-pol is much lower for the $HEM_{11\delta}$ mode). Simulated and measured reflection coefficient and radiation pattern for l_s = 2 mm and 8 mm are compared in Fig. 3.12 and Fig. 3.13 respectively. Increase in the cross-polar levels with l_s is clear from the radiation patterns. The mismatches in the resonant frequencies and the cross-polarization between simulated and measured results are due to the experimental errors.

Table 3.7 Measured performance of the microstrip fed CDRA for varying l_s

l_s (mm)	f_0 (GHz)	$\|\Gamma_{in}\|$ (dB)	% Band width	Max. gain (dB)		Gain asymmetry (dB)	Max. H-plane cx-polar level (dB)
				E-plane	H-plane		
< 2	No coupling						
2	3.41	–56	6.3	5.39	4.61	0.78	–23
4	3.47	–18	6.4	5.44	4.15	1.29	–20
6	3.53	–20	6.6	5.65	4.09	0.56	–19
8	3.59	–21	6.7	5.99	4.95	1.04	–16

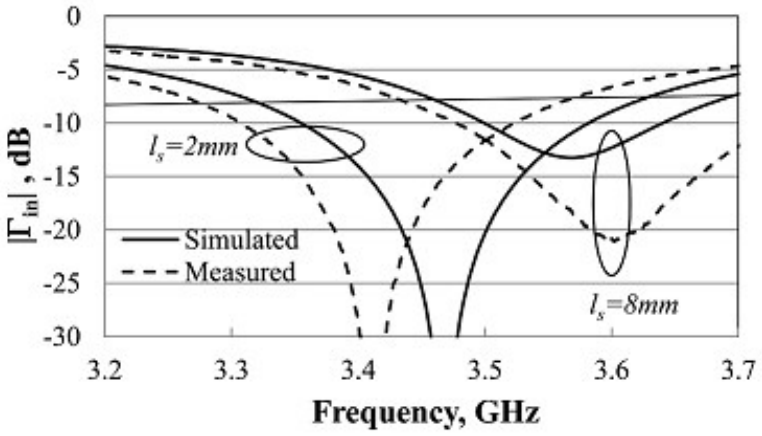

Fig. 3.12 Simulated and measured reflection coefficients of the microstrip fed CDRA for l_s = 2 mm and 8 mm

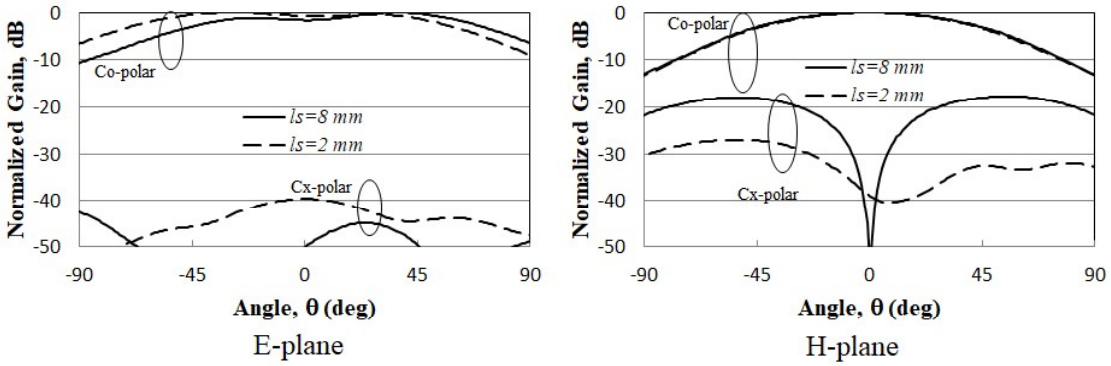

(a) Simulated

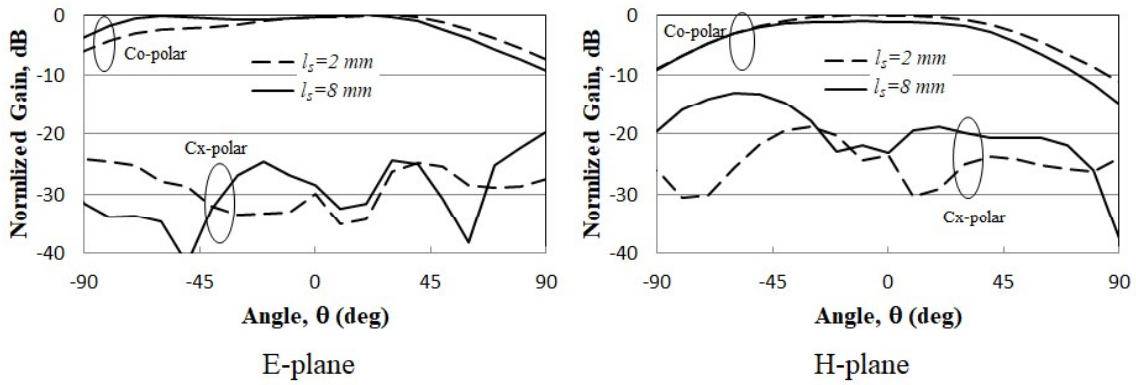

(b) Measured

Fig. 3.13 Radiation patterns of the CDRA for l_s = 2 mm and 8 mm. (a) Simulated (b) Measured

3.6 Feed perturbation and the dielectric constant of the CDR

Dielectric constant (ε_r) is a major design parameter of the CDRA that decides the resonant frequency of various modes of the DRA [8].

Table 3.8 Radiation characteristics of the CDRA for varying dielectric constants of the CDR (ε_r)

Dielectric constant, ε_r	**ε_r = 15**				**ε_r = 24**				**ε_r = 35**			
Feed index	1	2	3	4	1	2	3	4	1	2	3	4
Feed length, l_s (mm)	16	17	18	19	2	4	6	8	1	2	6	7
Res. frequency, f_0 (GHz)	3.95	3.98	4	4.04	3.47	3.52	3.55	3.57	3.07	3.09	3.17	3.17
Refl. coeff., $\|\Gamma_{in}\|$ (dB)	−19	−26	−38	−25	−50	−24	−35	−13	−24	−14	−16	−48
% Bandwidth	8.55	9.75	10.76	9.76	6.49	6.81	6.67	3.92	5.31	5.2	5.38	5.01
Pattern asymmetry (dB)	2.52	2.42	2.32	2.38	0.7	0.63	0.64	1.62	0.16	0.1	0.27	0.56
H-plane cx-polar level (dB)	−31	−27	−25	−23	−27	−26	−24	−19	−27	−24	−23	−19

It is well known that high dielectric constant DRs ($\varepsilon_r >> 10$) are easier to be excited with a microstrip [4], [19] but often radiates over a smaller bandwidth, as compared to lower dielectric constant (ε_r) of DRs. Even though the effect of ε_r in deciding the impedance matching, bandwidth and gain of the DRA are well known [4], the role of ε_r on the radiation purity of the CDRA under feed perturbation is little known. For this, HFSS simulations are performed for three different values ε_r = 15, 24 and 35 for the CDR ($2a$ = 19.43 mm, h = 7.3 mm). For each CDR, four matching lengths of the microstrip (l_s) for fair impedance matching with input reflection coefficient $|\Gamma_{in}| \leq -13$ dB are identified. These matching lengths are indicated using a feed index in the range 1 to 4. Corresponding radiation characteristics are extracted and are compiled in Table 3.8. From Table 3.8, it is clear that any given ε_r, the cross-polar level increases with l_s as expected. The trend in the pattern asymmetry is however different for low and high ε_r regimes, and it is very high for ε_r = 15. This is attributed to the fact that the above analysis is done for a fixed ground plane of 115 mm side for all the dielectric constants. Ground planes of large electrical size produce ringing in the E-plane pattern due to edge diffraction, that increases the gain / pattern asymmetry [45]. This asymmetry caused by the ringing effect is much more prominent than that caused by the higher order modes. For the present case, the ground sizes in terms of the free-space wavelength at the resonant frequencies are $1.53\lambda_0$ (~ 4 GHz for ε_r = 15), 1.34 λ_0 (~3.5 GHz for ε_r = 24) and $1.15\lambda_0$ (3 GHz for ε_r = 35) respectively. Hence unless the ground size is optimized for each case to eliminate the ringing, a conclusion can't be drawn on the dependence of pattern asymmetry on the ε_r.

3.7 Conclusion

This chapter presented an investigation on the feed perturbation effect of a CDRA excited in the $HEM_{11\delta}$ mode, on the basis of impedance and the radiation performances. This study revealed that if the feed point of the CDRA is optimized solely for impedance matching, then the higher order modes of the CDRA may also be excited which in turns deteriorate the CDRA performance. The threatening higher order mode was identified as a hybrid of the $HEM_{21\delta}$ and the $TM_{01\delta}$ modes of the CDRA. Three standard feed mechanisms were investigated both numerically and experimentally to understand the feed perturbation effect for a given feed type, and also that among the feeds. It was observed that shorter the matching length of the feed,

smaller the feed perturbation and higher the modal purity (symmetric radiation pattern with minimal cross-polarization). The cross-polarization was more correlated to the feed perturbation. But the pattern asymmetry is much more prominent in lower dielectric constant CDRAs due to edge diffraction effect. Thus, a smaller feed length is suggested for DRAs employing any feed mechanism for improved radiation performance. In the next chapter, investigations on the radiation characteristics of the $HEM_{21\delta}$-like higher order mode of a CDRA will be carried out with the purpose of inventing possible mitigation technique(s).

This document was created with the Win2PDF “print to PDF” printer available at
http://www.win2pdf.com

This version of Win2PDF 10 is for evaluation and non-commercial use only.

This page will not be added after purchasing Win2PDF.

http://www.win2pdf.com/purchase/